

MULTI-CLASS PLANT DISEASE CLASSIFICATION AND STAGE-WISE SEVERITY PREDICTION BASED ON MULTI-CLASS LEAF LABELLING

D.LITA PANSY¹, M.MURALI²

¹Department of Computer Science and Engineering, SRM Institute of Science and Technology,
Kattankulathur, India

²Department of Computing Technologies, SRM Institute of Science and Technology, Kattankulathur, India

E-mail: ¹ld5358@srmist.edu.in, ²muralim@srmist.edu.in

ABSTRACT

Plant Disease Severity Prediction (PDSP) aids in increasing the yield of a plant. However, research has been done scarcely on the severity prediction of multi-class Plant Disease (PD). Hence, this paper proposes multi-class leaf labeling and Exponential Pareto Fuzzy (EP-Fuzzy) based disease severity prediction. Primarily, input images with the complex background are taken and the background is removed in those images. The obtained background-removed images are utilized for increasing the dataset via augmentation and providing labeled data for the leaf labeling model utilizing augmented images. The unlabelled images are labelled in the Spearman-based Pseudo Labelling (S-PL) model by utilizing the augmented images. The labelled images and saliency-mapped images are fused to enhance the Segmentation Accuracy (SA) of Seam Carving-Region Split and Merge (SC-RSM). Afterward, the Depth-wise ResNet-50 (DRN) classified the class of the leaf diseases, with the segmented image and extracted feature. By utilizing the EP-Fuzzy model, the severity stage is predicted for the classified diseased leaf. The proposed technique's performance is experimentally assessed, where the proposed one exhibited superior performance on accuracy, training time, overall prediction rate, Dice Similarity Coefficient (DSC), et cetera.

Keywords: *Plant Disease Severity Prediction (PDSP), Multi-class Leaf label, saliency mapping, Spearman-based Pseudo labelling (S-PL), Depth-wise ResNet-50 (DRN).*

1. INTRODUCTION

Since plant crop yields are the main sources of food, fodder, and fuel, a doubling of the present global plant crop productivity is expected to be required by 2050, considering the population growth rate of recent years [1]. However, PDs, which are caused by various pathogens like pests, bacteria, or fungi that damage plant growth [2], are becoming a major obstacle in achieving the expected productivity. Most plants display visible symptoms in the leaves [3], while plants produce food through leaves. Thus, detecting PD and predicting its severity on the plant leaves not only aids in preventing the plant from dying but also can reduce the cost of using fungicides for dying crops. However, it is challenging to predict and classify leaf disease manually. Even experienced farmers often could not successfully detect certain PDs, which resulted in wrong conclusions and treatment

methods [4]. During severity estimation in leaves, images could be categorized into 2 different problem formulations, namely (1) Disease detection to detect the type of disease and (2) Disease quantification: defined as the extent to which an individual leaf has been affected [5]. Therefore, for disease detection and severity prediction in PDs, various Machine Learning (ML) models have been developed in recent years. For instance, to predict the leaf severity of Soybean rust, wheat leaf blast, *Nicotianatabacum-Xylellafastidiosa*, *Calonectria* leaf blight, and potato late blight, boosted regression tree models were developed [6].

In general, the PD severity index is utilized during the disease severity estimation. The "area of a sampling unit (plant surface) affected by disease expressed as a percentage or proportion of the total area" is named PD severity index [7] With this severity index model, severity estimation models were developed by numerous studies. Moreover,

segmentation techniques, namely threshold-based and clustering-based segmentation were utilized for diseased area recognition. Yet, the image background frequently encloses elements similar to the leaves and disease spots' representation in complex environments, which makes it complex for the recognition model for segmenting leaves and disease spots [8]. Moreover, the prediction was made with imaging techniques like spectral images [9] and visible light images. Nevertheless, this technology could not be applied extensively since the equipment used to acquire spectral images is expensive and difficult to carry [10]. Furthermore, the classification results could be misclassified owing to intra-class similarity. To resolve these issues, this paper proposes the EP-Fuzzy-based leaf disease stage-wise severity prediction with multi-leaf labelling.

1.1 Motivation of the study

The cultivation of fruits and vegetables holds a noteworthy position in the agriculture sector, making a substantial contribution to the economy and serving as a crucial means of subsistence for numerous farmers across the globe. The presence of diseases in the plants reduces the growth of vegetables and fruits. Hence, a precise identification system is needed for efficient management of the agriculture sector. Many research studies are focused on the leaf disease classification for further treatment of the plant. However, some research works focus on specific plants in disease monitoring. Similar to existing research by [11], this research only concentrated on the multiclass classification of grape leaf, which was only helpful for grape cultivation. Also, existing research by [12] did not concentrate on the plant disease severity assessment, which reduced the efficiency of the disease monitoring for treating the plants. So, this proposed research work intends to present the multi-leaf disease identification and severity identification system using advanced methods.

1.2 Problem statement

The problems detected in the existing PDSP models are given as follows,

- The fine-grained disease severity classification is more challenging owing to the large intra-class similarity among the multi-class plants.

- Most of the existing research failed to focus on multi-class disease recognition in a single leaf, as there is a possibility that more than one disease may be exhibited in a single leaf.
- The background subtraction techniques in the existing severity prediction models might not be suitable for complex backgrounds.
- Training the classifier with fewer data causes the over-fitting problem, which classifies the trained data accurately but cannot classify the new test data.

Hence, to avoid these problems in the proposed framework, the following contributions are made.

- To differentiate the multi-leaf classes, semi-supervised S-PL-based leaf labeling is performed. If the classifier is only trained with the features of diseases, then misclassification might be presented. Hence, the leaf images are labeled.
- To predict the multi-class disease in a single leaf, the SC-RSM segmented multi-disease features were utilized to train the multi-disease prediction classifier. Detection of multi-classes diseases in a single leaf might be helpful in managing diseases more effectively, preventing the spread of the disease to the other parts of the leaf and enabling targeted treatment to prevent the plant disease.
- To subtract the leaf complex background, the N-GMM-based background removal is proposed. The background of the leaf image might increase the error rate in the disease prediction process. Hence, the background of the leaf image is removed.
- To enhance the quality of the prediction model, the input data for training has been increased by using data augmentation. If diverse data is presented during the testing process, then the classification error outcome might be presented. Hence, the data augmentation process is highly concentrated.

The remaining paper is systemized as: the related works are exemplified in Section 2. Section 3 explicates the proposed methodologies. The outcomes are delineated in Section 4. Lastly, the paper is wrapped up in Section 5.

2. RELATED WORKS

2.1 The Survey Related To Plant Leaf Disease Severity Identification

[13] established a deep learning architecture for the classification of plant leaf disease and severity prediction. First, the images were preprocessed to extract better features. The features were extracted and given to the Convolutional Neural Network (CNN) classifier, which classified the disease type in the tomato plant. The severity level was then identified based on the respective classes, such as bacterial spot, early blight, spider mites, mosaic virus, and yellow leaf. Hence, the severity of the plant disease with respect to the classified disease was predicted accurately. However, only the tomato plant disease was considered, which needed further plant disease classification for better results in disease prediction.

[14] developed disease severity identification in mangrove leaves with hyperspectral imaging spectroscopy. The input image was smoothed with a Savitzky-Golay (SG) smoothing filter. The spectral and textural features were extracted and the optimal features were selected using the Successive Projection Algorithm (SPA). The severity of the disease was then identified using Random Forest (RF) by visualized mapping of the image. Hence, the disease severities in mangrove leaves were estimated regarding traits of the leaves. Yet, the background of the image was not removed, which detected the normal leaf as a diseased leaf.

[15] implemented severity prediction of leaf disease regarding chlorophyll content of the leaf. The image of each leaf sample with the gray panel was obtained utilizing SOC710 hyper-scanner data acquisition and then smoothed by an SG filter. Next, the Soil Plant Analysis Development (SPAD) value was estimated. Then, by using the SPA method, the diseases in the leaves were mapped regarding SPAD value. Hence, with the help of a mapped image, the severity of the leaf disease was predicted precisely. On the contrary, only a few image data were taken for the disease severity prediction. Thus, large data could not be analyzed by this model.

[16] evaluated plant disease prediction in wheat leaf through plant leaf extract and bio-agent. The leaf extracts, such as Neem extract and Moringa extract were used as an examination tool for leaf disease prediction. The Foliar treatment was done for the

wheat sampling using the two extracts. Then, with the help of a spectrophotometer, the chlorophyll content of the plant was calculated. Then, the severity of the disease in leaves was statistically analyzed using the ANOVA (Analysis of variance) test regarding the chlorophyll content. Thus, the impact of the extracts on leaf disease prediction was found. However, the bio-agents used could not resist the wheat loss, which would affect the model in input collection.

[17] evaluated multiclass classification and severity prediction of the chili leaf disease using the EfficientNetB4 method. The input image was first preprocessed for noise removal, image enhancement, and data augmentation. Then, the image was classified using the customized deep learning network EfficientNetB4. Also, with the customized classifier, the severity of the plant disease was predicted. Thus, the chili leaf disease was predicted accurately by this method. But, important features were not extracted for disease prediction, which led to the misclassification of the plant leaf disease.

[18] employed a two-stage Deep Learning (DL)-centric segmentation model for crop disease quantification of corn leaves. For segmentation, UNet, SegNet, and DeepLabv3+ network architectures were utilized by the model. During testing, the severity of 3 disease classes very close to the actual observations was predicted by the UNet-DeepLabv3+ model. However, the models were trained with fewer images, which would induce the curse of dimensionality issue.

[19] suggested adaptive thresholding of Convolution Neural Network (CNN) features of maize leaf images for severity estimation. The Regions Of Interest (ROI) were extracted by the adaptive thresholding; then, the leaf disease severity was estimated with the ROI. As per the experimental outcomes, transfer learning systems classified diseases with a higher accuracy level. Yet, the model did not consider the background of the leaf, which would deviate the classifier's accuracy.

[20] estimated the severity of grapevine diseases with a fuzzy inference system. For estimating the severity, the fuzzy model considered the lesion spots and the symptomatic area. The fuzzy model's performance analysis revealed that the best outcomes were yielded by the automatic estimation of symptom severity. However, the Degree Of

Membership (DOM) might overlap with the used membership function.

[21] implied maize common rust severity prediction grounded on automatic fuzzy logic. The disease severity was predicted with CNN DL models, which leveraged images segmented utilizing a threshold. As per the outcomes, the VGG16 model reached the testing accuracy of 89% on common rust disease images. Nevertheless, the model working on the complex background is questionable since it was trained with plain background images.

[22] propounded a residual network with an attention system for PDS detection. Here, the enhanced channel as well as spatial attention module were embedded into the ResNet's residual block. By doing so, the model attained better accuracy for multiple and single PDS classification. But, the residue block with the attention module might not be optimal.

2.2 The Survey About Plant Disease Classification

[23] propounded a lightweight CNN network for PDS recognition. A building block with Channel Shuffle operation and Multiple-Size module (CSMS) was developed by the network. The experiential assessment exposed a high accuracy level, which exemplified the PD diagnosis's efficacy. Nevertheless, the lightweight CNN's performance was not as satisfactory as the conventional ResNet model.

[24] employed Fuzzy C-Means-centric Chameleon Swarm Algorithm (FCM-CSA) for PD classification. The PDs were detected with the Progressive Neural Architecture Search (PNAS). During the experimental analysis, the PNAS model outperformed in PD classification. Yet, the child's networks could not be assessed or trained in the PNAS model.

[25] instigated PD detection with the hybrid model, which was grounded on Convolutional Auto-Encoder (CAE) and CNN. The CAE-CNN model decreased the time required for training a model for automatic PD detection. Yet, the non-linear activation in the pooling process could cause a vanishing gradient problem in the CNN model.

2.3 The Survey On Single Plant-Based Disease Identification

[26] established a DL-centric evaluation of disease severity for early blight in tomato crops. A deep ResNet101 was utilized to predict the early blight disease severity in tomato leaves. During the experimental evaluation, the ResNet101 reached the maximum accuracy level (94.6%) during severity prediction. Yet, the classifier's training time was increased by more deep layers.

[27] proffered a severity estimation system for tomato generic diseases. For disease detection, ResNet learned to detect instances of disease grounded on generic features; also, for the severity prediction, UNet was utilized. The implementation outcomes displayed how the leaf properties impacted disease detection. Nevertheless, the segmented results are less accurate when contrasted with the ground truth images.

2.4 Contribution and Key Hypothesis

In this work, multiple plant leaves were considered for disease classification. This is because the type of disease and characteristics vary for each plant. The existing works have not classified the disease for multiple plant leaves classification. The plant leaves would contain several diseases; so, in this research, multi-disease is taken for the severity prediction of the leaf disease. Also, in this work, four kinds of plants, such as corn, mango, tomato, and soya are considered. To make the prediction performance accurate, the input image background is extracted and labeled. This helps in identifying the types of disease present in plant leaves. Also, the proposed classifier classifies large data accurately.

This research implementation is done to show the efficiency of the proposed algorithms, which shows the expediency of the generated hypotheses. Also, the results illustrate that our proposed system can answer the research hypotheses, which were addressed from the previously published literature on a similar subject. This paper complements and supports the key hypotheses in the following ways:

- (1) Identifying the significant hypotheses from previous articles and making them into research problems.
- (2) Isolating the reasons behind significant hypotheses.

(3) Implementing the factors that form significant hypotheses.

2.5 Scope of this research

The identification of leaf disease and stage identification will be helpful in treating the plant to reduce the spread of the disease in other parts of the plants. Hence, the leaf diseases are identified in the leaf. However, none of the existing research works concentrated on multi-leaf plants, such as corn, mango, tomato, and soya plants for multi-disease prediction and stage identification. Also, most of the existing research works didn't concentrate on the proper handling of input data in terms of background removal, data diversity, and segmentation. Hence, this research work presented the S-PL-based leaf labeling, EF-Fuzzy-based severity identification, and DRN-based disease prediction. Also, the N-GMM-based background removal process and SC-RSM-based segmentation process are carried out to increase the classification performance.

3. PROPOSED PLANT DISEASE SEVERITY PREDICTION METHODOLOGIES

The major factors influencing food production are the PDs caused by pathogens. Disease classification and severity prediction in leaves are becoming a complex process owing to the rough background and high intra-class similarity. Hence, to overcome these issues, this paper proposes a leaf labeling-based multi-disease classification and EP-Fuzzy based severity stage prediction, which is exemplified in Figure 1,

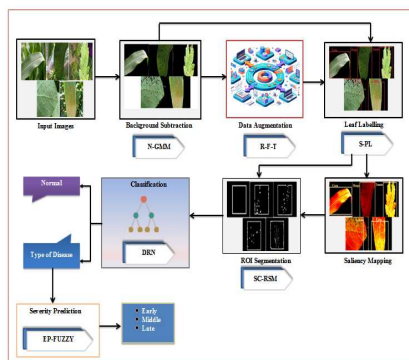


Figure 1: Block representation of the proposed model

3.1 Input data

Primarily, for the PDSP, the healthy and diseased leaves of corn, mango, soybean, and tomato are taken with their corresponding classes. The input dataset (D) is mathematically expressed as,

$$D = \{d_1, d_2, \dots, d_n\} \text{ or } d_\alpha, \alpha = 1, 2, \dots, n \quad (1)$$

Where, the n^{th} image is signified as d_n . In the given dataset, 5% of data (d_α) is utilized as labeled data of corn (cr), tomato (tm), mango (mg), and soya (sy) plant leaves, which is given in a separate class ($d_\alpha \in D$).

3.2 Background Subtraction

The individual is separated from the background using the Normalized-Gaussian Mixture Model (N-GMM) since the given input data contains a rough background. The Gaussian Mixture Model (GMM) is considered in the proposed model as it can automatically recognize the subpixels of the foreground image. However, the GMM model struggles with the pixel values, which are not normally distributed. Hence, to solve this problem, Normalization is introduced when the pixels are distributed, and the technique is named N-GMM.

Step 1: Primarily, the pixels in the image d_α are represented as $[p_1, p_2, \dots, p_q]$ or p_w . Afterward, these pixels are normalized using,

$$\bar{p}_w = \frac{p_w - \min(p_w)}{\max(p_w) - \min(p_w)} \quad (2)$$

Where, \bar{p}_w implies the normalized pixel value, and $\min(p_w), \max(p_w)$ elucidate the maximum and minimum pixel values.

Step 2: Thereafter, from the normalized pixels \bar{p}_w , the GMM models the background pixel using a mixture of N Gaussian distribution. At the time τ , the probability (ρ) of observing a background pixel ($p_\tau \in d_\alpha$) is the weighted sum of N distributions, which is depicted as,

$$\rho(p_\tau) = \sum_{k=1}^N w_{k,\tau} * \zeta(p_\tau, \delta_{k,\tau}, v_{k,\tau}^2) \quad (3)$$

Where, $w_{k,\tau}, \delta_{k,\tau}, v_{k,\tau}$ exemplifies the weight, mean value, and variance matrix of the k^{th} distribution at the time τ , and ζ defines the probability density function of k^{th} distribution, which can be represented as,

$$\zeta(p_\tau, \delta_{k,\tau}, v_{k,\tau}^2) = \frac{1}{\sqrt{2\pi v^2}} \exp\left(-\frac{(p_\tau - \delta)}{2v}\right) \quad (4)$$

Where, (δ) is the mean value, and (v) is the variance matrix. Afterward, to avoid complex matrix evaluation, the red, blue, and green pixels have the same variance such that,

$$v = (sd)^2 \cdot \mathcal{I} \quad (5)$$

Here, sd, \mathcal{I} specifies the standard deviation and identity matrix, correspondingly. In this way, the background is modeled.

Step 3: When a new pixel $p_{\tau+1}$ comes, it is checked with existing N distributions until a match is found, and the match is represented as,

$$|p_\tau - \delta_{k,\tau}| \leq t \quad (6)$$

Where, t is a threshold constant. When no match is found, then a new distribution is created with current p_τ as the δ value. Moreover, the weight $(w_{l,\tau})$ is adjusted as,

$$w_{l,\tau} = (1 - \eta)w_{l,\tau-1} + \eta\psi_{l,\tau} \quad (7)$$

While η is the learning rate, ψ symbolizes the match calculated, where ψ is one if the match is found, else ψ is zero. After every updation procedure, the N distributions are estimated by the value (w/sd) . Also, the top of the N distributions is considered as the probable M background distribution, which is represented as,

$$M = \arg \min \left(\sum_{l=1}^m w_{l,\tau} > t \right) \quad (8)$$

Where, m implies the number of background distributions and $(\arg \min)$ is the minimum argument function.

Step 4: Afterward, from the image d_α , the background distributed pixels are removed and the foreground is obtained. The image after the background removal is notated as f_α .

3.3 Data augmentation

For increasing the dataset size and for training the labeling process, all the labeled images of corn (cr), tomato (tm), mango (mg), and soya (sy) plant leaves in the dataset are given for augmentation. The input images for disease classification are augmented by the Rotation Flipping Translation (R-F-T) process.

Rotation: First, the rotation on four angles $(+90^\circ, -90^\circ, +270^\circ, -270^\circ)$ is performed to augment the image data $f_\alpha = Rot$.

Flipping: Two types of flipping, namely horizontal flipping and vertical flipping are performed on $f_\alpha = Flp$ to create augmented data.

Translation: During the translation of the image $f_\alpha = Tr$, the images are moved in the x-axis and y-axis by +10 and -10 pixels to augment the dataset.

After the augmentation process, the f_α images are augmented to nx images using the augmentation techniques $(aug = Rot, Flp, Tr)$. Therefore, the augmented set is exemplified as $B = \{f_{aug(nx)}, aug = Rot, Flp, Tr\}$.

The number of images present before augmentation and after augmentation are given in Table 1,

Table 1: Augmentation details

Images	Before Augmentation	After Augmentation
Total	1965	5895
Training	1572	4716
Testing	393	1179

3.4 Leaf labeling

After the images are augmented, the leaf label is created with the proposed Spearman-based semi-supervised Pseudo-Labeling (SPL) model. As Pseudo Labeling (PL) creates the most appropriate labels for images only with a few labeled data, it is considered for leaf labeling. However, with the existing PL technique, the decision boundary might be over-trained, which might create mislabeled output. Hence, to solve this problem, the distances between two instances are estimated using the Spearman technique.

Here, to avoid misclassification of leaf diseases, the labeling is performed because, if the classifier is trained only with the features, similar features in leaf disease, such as spots in tomatoes may be classified as the spot disease in soybean or mango. Hence, to avoid this misclassification, the labeling of leaf images is performed.

In the proposed model, the labeled augmented data of corn (cr), tomato (tm), mango (mg), and soya (sy) plant leaves are utilized as the labeled data (B) of the PL model, which is specified as,

$$B = \{B_{nn}, nn = cr, tm, mg, sy\} \quad (9)$$

With the labeled images as a reference, 95% of the unlabeled data after background subtraction can be labeled with the proposed SPL model. The unlabeled image data (UD) is expressed as,

$$UD = \{K_1, K_2, \dots, K_{n'}\} \text{ or } K_{ul}, ul = 1, 2, \dots, n' \quad (10)$$

Where, $B_{nn}, K_{nn'}$ illustrates the nn^{th} and nn'^{th} labeled and unlabeled image. The labeled and unlabeled image instances are clustered

differently during training in the SPL model. For the images with labels (B_{lab}), the traditional supervised learning model is used, where the cross-entropy loss is calculated by comparing the predicted label with the given label as,

$$\xi = - \sum_{lab=1}^{nn} B_{lab=cr,tm,mg,sy} \log(o_{lab}) \quad (11)$$

Where, ξ implies the cross entropy loss value, and o_{lab} specifies the output labeled image. If the loss value is small, then the output o_{lab} is grouped into a cluster by estimating the Spearman correlation coefficient (σ).

Pseudo-label is wielded in the fine-tuning phase of the same supervised model with dropout. The pre-trained network is given with labeled as well as unlabeled images concurrently to predict the pseudo-labels by minimizing the total loss (ℓ), which is the weighted sum of labeled and unlabeled image data as,

$$\ell = \frac{1}{nn} \sum_{lab=1}^{nn} \sum_{g=1}^c \xi(o_{lab}^g, \lambda_{lab}^g) + \varpi(b) \frac{1}{n'} \sum_{ul=1}^{n'} \sum_{g=1}^c \xi(o'_{ul}^g, \lambda'_{ul}^g) \quad (12)$$

Where, n, n' specify the number of labeled and unlabeled images, and C represents the number of classes, which is the number of clusters required. In the proposed model, the value of C is given as 4.

$\varpi(b)$ is the coefficient balancing the labeled and unlabeled image features, $o_{lab}^g, \lambda_{lab}^g$ is the output and corresponding label of the labeled image, and $o'_{ul}^g, \lambda'_{ul}^g$ signify the output of the unlabelled image and its corresponding predicted pseudo-label. The o'_{ul} is estimated with the class having the maximum predicted probability, which is given as,

$$o'_{ul} = \begin{cases} i = \text{argmax}(\lambda'_{ul}) & \text{if } o'_{ul} = 1 \\ \sigma & \text{otherwise} \end{cases} \quad (13)$$

Here, the decision boundary's objective is computed based on the Spearman distance, which is given as,

$$\sigma = 1 - \frac{6 \sum_{i=1}^n \mathfrak{R}_i^2}{n(n^2 - 1)} \quad (14)$$

Where, σ illustrates the Spearman correlation coefficient, which is the decision boundary, \mathfrak{R} epitomizes the distances between two image instances $(B_{lab=cr,tm,mg,sy}, K_{ul})$, where, r symbolizes the random number.

Let $\varpi(b)$ signifies the coefficient balancing the labeled and unlabeled image features at the epoch T . If $\varpi(b)$ is too high, it disturbs the training to label the images; thus, the $\varpi(b)$ is slowly increased after some epochs as,

$$\varpi(b) = \begin{cases} 0 & \text{if } b < \lambda_1 \\ \frac{b - \lambda_1}{\lambda_2 - \lambda_1} \varpi_\lambda & \text{if } \lambda_1 \leq b < \lambda_2 \\ \varpi_\lambda & \text{if } \lambda_2 \leq b \end{cases} \quad (15)$$

Where, λ implies the training epochs, and ϖ_λ is the output balance parameter value. After performing these processes, the labeled leaf image dataset $(I_{cr,tm,mg,sy})$ is obtained, which is expressed as,

$$I_{cr,tm,mg,sy} = \{i_1, i_2, \dots, i_z\} \text{ or } i_\kappa, \kappa = 1, 2, \dots, z \quad (16)$$

Where, the z^{th} labeled leaf image is notated as i_z . The image (i_κ) is now given for mapping as shown below.

3.5 Saliency mapping

After the multi-class leaf images are labeled, the diseased areas are created as a map using the saliency mapping model. This is done to solve the challenging threshold selection and contour selection in the prevailing segmentation techniques. The steps of saliency mapping are given as,

Primarily, the spatial features, such as color, orientation, and intensity in the images are extracted and a discrete visual fixation map (F_κ) is created for the image i_κ as,

$$F_\kappa(\vec{k}) = \sum_{u=1}^A \partial(\vec{k} - \vec{k}_F(u)) \quad (17)$$

Where, \vec{k} describes the vector representing the spatial coordinates in i_κ , $\vec{k}_F(u)$ specifies the spatial coordinates of u^{th} visual fixation (i.e., diseased region), A is the number of visual fixation in i_κ .

Thereafter, the saliency map $(\zeta(\vec{k}))$ is obtained by convolving the fixation map with a Gaussian function $(\Theta(\vec{k}))$ as,

$$\zeta(\vec{k}) = F(\vec{k}) * \Theta(\vec{k}) \quad (18)$$

Hence, the final saliency-mapped image is elucidated as \mathfrak{S}_κ , and this image is fused with (i_κ) and used for classification as described in the following section.

3.5.1 Image fusion

After the saliency-mapped image \mathfrak{S}_κ is obtained, it is fused with the corresponding leaf-labeled image (i_κ) . This process is done to enhance the features of the diseased region (ROI) in the leaf images. The image fusion is given as,

$$S_\kappa = \mathfrak{S}_\kappa \oplus i_\kappa \quad (19)$$

Where, S_κ specifies fused image. Here, the images (\mathfrak{S}_κ) and (i_κ) are fused by combining these images. The fusion of both images is represented by the (\oplus) operator.

3.6 ROI Segmentation

After the fused image (S_κ) is obtained, the ROI in the images is segmented for training the disease features to the classifier. Here, the ROI is segmented with the SC-RSM algorithm. The Region Split and Merge (RSM) is considered as it splits the image into quadrants grounded on the homogeneity criterion and homogeneous regions are merged to give the segmented result. By doing this, the most accurate segmentation of ROI can be

obtained. Nevertheless, the RSM has limitations in defining the homogeneity criterion. Therefore, to overcome this problem, the Seam Carving (SC) model is introduced in RSM segmentation.

(i) Primarily, the image (S_κ) is split into regions, such as 4×4 matrix format. The split image regions are represented as,

$$S_\kappa = \{s_1, s_2, \dots, s_m\} \text{ or } s_\varepsilon, \varepsilon = 1, 2, \dots, m \quad (20)$$

Here, the m^{th} split region is given as s_m .

(ii) Then, the homogeneity is checked with SC as,

- Initially, the pixels in s_ε are given an energy value. Here, the highest energy value (E) is taken as the intensity level of the saliency-mapped image. By doing this, the ROI will have the highest energy, whereas healthy leaf parts will have lower energy.

$$E = \max(s_\varepsilon) \quad (21)$$

- Afterward, a path is created from the top of the image s_ε to the bottom of s_ε with the least energy pixels. This is done by creating eight connected lines to the neighboring pixels with low energy. By doing this, all the pixels with low energy will create a path.
- Next, all the pixels in the path are deleted. This aids in removing the pixels in the healthy region in the image.

By doing this, the homogeneity in s_ε will be obtained, which is ROI pixel intensity. After homogeneity identification, the image region is represented as,

$$s_\varepsilon \rightarrow y_\varepsilon \quad (22)$$

Where, (y_ε) is the homogeneity identified image.

(iii) Repeat the homogeneity criterion on every single partitioned region. Thereafter, this homogeneity is checked with neighbor regions $(y_{\varepsilon+1})$.

(iv) If the two regions $y_\varepsilon, y_{\varepsilon+1}$ have homogenous intensity, two regions are merged using the operator (\otimes) as,

$$T_\kappa = y_\varepsilon \otimes y_{\varepsilon+1} \quad (23)$$

Where, (T_κ) is the segmented image.

(v) Else, repeat steps (iii) and (iv) until all regions are merged.

After all the images are merged, the resultant segmented image is given T_κ . The segmented regions might also be multi-disease in a single leaf. Therefore, with the proposed model, multi-disease features from a single leaf can be utilized to train the classifier, which could predict multi-disease in a single leaf.

3.7 Feature extraction

After the ROI segmented image (T_κ) is obtained, features, such as orientation extent features, which are challenging feature mapping of the classifier, are extracted. Along with that, the features, including rotation, 3D viewpoint, illumination, correlation, homogeneity, extended orientation, Grey Level Co-occurrence Matrix (GLCM), and Histogram of Gradients (HOG) are extracted from T_κ . For extracting the rotation feature of the image, the (T_κ) is transformed along the x and y axes. It is defined as,

$$\begin{bmatrix} P \\ Q \end{bmatrix} = \begin{bmatrix} \cos \phi & -\sin \phi \\ \sin \phi & \cos \phi \end{bmatrix} \begin{bmatrix} p \\ q \end{bmatrix} \quad (24)$$

Where, P, Q denotes the new coordinate of (T_κ) after rotation, x, y imply the initial image coordinates of (T_κ) , and ϕ implies the rotation angle. The feature 3D viewpoint of (T_κ) is derived as follows,

$$T_3 = \frac{x - (a_1)}{u} = \frac{y - (a_2)}{v} = \frac{z - (a_3)}{w} \quad (25)$$

Where, T_3 indicates the 3D viewpoint, x, y, z denote the three axes of (T_κ) , u, v, w imply the 3D view coordinates of (T_κ) , and a_1, a_2, a_3 specify the 3D pixel coordinates of (T_κ) . The illumination (I_ℓ) of (T_κ) is detected based on the measure of visible light or luminance flux in the image. It is evaluated by,

$$I_\ell = L_{\max} \int \mathfrak{R}_s e(\lambda) \Delta \lambda \quad (26)$$

Where, L_{\max} denotes the maximum luminance, \mathfrak{R}_s indicates spectral radiance, $e(\lambda)$ implies luminance efficiency, and $\Delta \lambda$ specifies wavelength interval. Hence, the luminance is extracted from (T_κ) .

Further, the correlation feature is extracted by the pixel intensity and grayscale value of (T_κ) . It is evaluated by,

$$T_{cor} = \frac{\sum_c \sum_d [f(c, d) - \hat{f}] [g(c, d) - \hat{g}]}{\sum_c \sum_d [(f(c, d) - \hat{f})^2 \times (g(c, d) - \hat{g})^2]} \quad (27)$$

Where, $f(c, d)$ denotes the pixel intensity of (T_κ) at (c, d) coordinates, $g(c, d)$ indicates the grayscale value at (c, d) coordinates, \hat{f}, \hat{g} imply the average values of intensity in f, g , respectively. The GLCM specifies the information regarding pixel position of (T_κ) that had a similar amount of gray levels. It is extracted by,

$$G_d[a, b] = n_{a,b} \quad (28)$$

Where, G_d indicates the co-occurrence of the image pixel matrix and $n_{a,b}$ denotes the number of pixel co-occurrence at a, b gray levels. For extracting HOG, the T_κ is initially compressed to a 1:2 ratio of height and width accordingly. Then, the pixel gradients of T_κ are determined along both the x and y directions. Further, from the gradients, the

orientation and magnitude of pixels are estimated by using Pythagoras theorem. Subsequently, the histogram of T_κ is extracted.

The Homogeneity of T_κ is extracted based on the similarity of characteristics between the pixels of the image. The lower variance among pixels demonstrates the higher homogeneity of T_κ . Thus, the significant features are extracted for disease classification, which is mathematically depicted as O .

3.8 Disease classification

Afterward, the extracted features (O) and the segmented image T_κ are given as input to the Depth-wise-ResNet-50 (DRN). Here, the ResNet-50 (RN) is considered since it can process image data effectively and create fewer error values. However, the RN has a limitation of higher training time. Thus, to solve this issue, the transposed convolution layers in RN are replaced by the depth-wise convolution operation. Figure 2 displays the DRN architecture,

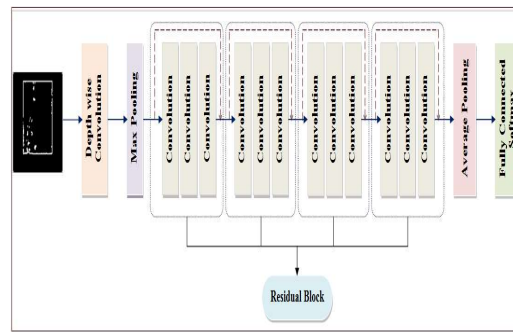


Figure 2: Architecture of DRN

Input: The input of DRN is the combination of O and T_κ , which is symbolized as \mathfrak{T}_κ . The DRN consists of convolution layers, which perform depth-wise convolution, max-pooling layers, and fully connected layers with the neurons activated with softmax function.

Depth-wise convolution: Primarily, the depth-wise convolution takes place in the DRN in which it uses a kernel (μ) of size $\hat{h} \times \wp$, where, \hat{h}, \wp indicates

the row and column size of the kernel. Therefore, the convolution operation $(U(\cdot))$ is given as,

$$C_h = U(\mu, \mathfrak{S}_\kappa) = \sum_h \sum_\varphi \mu_{(h,\varphi)} \circ \mathfrak{S}_{\kappa(Z+h,Y+\varphi)} \quad (29)$$

Where, Z, Y depicts the row and column size of the image \mathfrak{S}_κ . After the feature maps are extracted in the depth-wise convolution layer, it is given to the Max-pooling layer. The image obtained after the h^{th} depth-wise convolution layer is signified as C_h .

Max-pooling layer: This layer reduces the dimension of the feature map in C_h by selecting the significant features. The max-pooling operation is expressed as,

$$P_{\max} = \max\left(\frac{C_h - \omega}{\Omega}\right) \quad (30)$$

Here, P_{\max} implies the max-pooled feature map, with the kernel ω , the stride length (Ω) , which decides the number of pixel shifts, by the kernel during feature mapping.

Residual block: The DRN uses a bottleneck residual block, which uses 1×1 convolution for reducing the matrix multiplications. The residual blocks perform convolution in such a way that a layer's output is taken and added to the output of another layer by skipping connections. There are several residual blocks, which map the features of P_{\max} by reducing the dimension and finding the important feature maps. The final residual block feature map output is specified as E_{res} .

Average pooling: Average pooling estimates the average feature map (U_{avg}) in the image E_{res} by,

$$U_{avg} = \frac{1}{|\Gamma|} \sum_{E_{res} \in \Gamma} E_{res} \quad (31)$$

Where, Γ illustrates the average feature map.

Output: The average pooled feature-mapped image is given to the fully connected layer, which utilizes softmax activation for predicting the output class of the given image. The softmax activation (\mathcal{G}) is given as,

$$\mathcal{G} = \frac{\exp(U_{avg})}{1 + \exp(U_{avg})} \quad (32)$$

The output classed image is specified as H . From the classified output, the severity level of the disease is identified using EP-Fuzzy as detailed in section 3.9. Table 2 exemplifies the hyper-parameters of the proposed DRN,

Table 2: Hyper-parameters of DRN

Hyper-parameters	Value
Input size	(32,32,3)
Optimizer	Stochastic Gradient Descent (SGD)
Loss Function	Cross Entropy
Classifier	Softmax
Epochs	30
Batch Size	128

Pseudocode of DRN

Input: segmented image $(T_\kappa), O$

Output: Classified class output

Begin

Initialize $(\mathcal{G}), \Omega$, kernel size, target accuracy (ta)

For each \mathfrak{S}_κ

If predicted accuracy $(pa \geq ta)$ {

Select pa

} **Else** {

```

        Perform depth-wise convolution  $\mu_{(h,\varphi)} \circ \mathfrak{I}_{\kappa(Z+h,Y+\varphi)}$  which the fuzzifier converts the crisp input to fuzzy input. The DSP index ( $\gamma$ ) is estimated as,
    
```

$$\gamma = \frac{V}{V+U} \times 100 \tag{33}$$

```

        Compute  $P_{\max} = \max\left(\frac{C_h - \omega}{\Omega}\right)$ 
    
```

Where, V,U implies the number of foreground (ROI) and background pixels, respectively. This γ is fuzzified using the Exponential Pareto (EP) membership function. The membership function (G) is given as,

$$G = \exp\left(1 - \frac{\gamma}{J}\right)^v \tag{34}$$

```

        Process residual blocks feature mapping
    
```

Here, J,v exemplifies the center and width of the fuzzy set.

```

        Perform  $\sum_{X \in \Gamma} X$ , and fully connected  $\mathcal{G}$  activation
    
```

Rules verification: For predicting the severity of the diseased leaves, a set of rules is generated to map the DOM function. Afterward, the rules are verified in the fuzzy inference process. The fuzzy rules for severity prediction are given as,

```

        End If
    
```

```

        End For
    
```

```

        Return Predicted class
    
```

End

The output of the DRN is the healthy leaf class or diseased leaf class. The DRN predicts the single diseased class and multiple disease classes in a single leaf image. The disease leaf classes for corn are Gray Leaf Spot, Leaf Blight, and Rust Leaf. For mango, the disease classes are Anthracnose, Phoma Blight, and Red Rust, and for soya, it is Bacterial Blight, Brown Spot, Cercospora Leaf Blight, and Soya bean Rust. For tomatoes, the disease classes are Early Blight leaf, Septoria Leaf Spot, Leaf Bacterial Spot, Leaf Late Blight, Leaf Mosaic Virus, Leaf Yellow Virus, and Mold Leaf. The predicted healthy classes are neglected and the single or multi-diseased plant classed image is given for PDSP.

3.9 Severity prediction

By utilizing the EP-Fuzzy, the disease severity in the diseased leaf image is estimated. Here, the fuzzy is selected as it predicts the more accurate results with the defined fuzzy rules. However, owing to the right spread, the membership function mapping in existing fuzzy might get overlapped. Thus, to overcome this problem, the Exponential Pareto function is used in the Fuzzy approach.

Fuzzification: Primarily, the crisp input of Disease Severity Percentage (DSP) is given as input in

$$Early = \begin{cases} \exp\left(\frac{\chi(\gamma - \Delta_1)}{\Delta_1 - \Delta_2}\right) & \text{if } \Delta_1 \leq \gamma \leq \Delta_2 \\ 1 & \text{if } \Delta_1 > \gamma \end{cases} \tag{35}$$

$$Mid = \begin{cases} 1 & \text{if } \Delta_1 > \gamma \\ \exp\left(\frac{\chi(\gamma - \Delta_1)}{\Delta_1 - \Delta_2}\right) & \text{if } \Delta_1 \leq \gamma \leq \Delta_2 \\ \exp\left(\frac{\chi(\gamma - \Delta_3)}{\Delta_3 - \Delta_4}\right) & \text{if } \Delta_3 \leq \gamma \leq \Delta_4 \end{cases} \tag{36}$$

$$Late = \begin{cases} 1 & \text{if } \Delta_5 \geq \gamma \\ \exp\left(\frac{\chi(\gamma - \Delta_5)}{\Delta_5 - \Delta_6}\right) & \text{if } \Delta_5 \leq \gamma \leq \Delta_6 \end{cases} \tag{37}$$

Where, *Early, Mid, Late* are the three disease severity stages in the diseased leaf, $\Delta_1, \Delta_2, \Delta_3, \Delta_4, \Delta_5, \Delta_6$ are the limits of the DSP, which has values of 1%, 25%, 26%, 50%, 51% and 100%. Therefore, with these rules, the DOM will be mapped, and the rules will be verified for each leaf. Afterward, the

rules are aggregated by combining the degrees of satisfaction level of the rules and then the fuzzy set (Q) is obtained.

Defuzzification: After Q is obtained, the fuzzy values are converted to crisp output in the defuzzification process. Here, the centroid of the fuzzy sets is obtained, which gives the defuzzified crisp severity stage (SS) of the PD.

Pseudocode of EP-Fuzzy

Input: Disease class leaf (H)

Output: Severity stage

Begin

Initialize fuzzy parameters $J, V, \Delta_1, \Delta_2, \Delta_3, \Delta_4, \Delta_5, \Delta_6$

For disease class H **do**

Estimate DSP with

$$\gamma = \frac{V}{V + U} \times 100$$

Fuzzify γ with EP function

Verify fuzzy rules

If ($\Delta_1 \leq \gamma \leq \Delta_2$) {

Map DOM as *Early*

using $\exp\left(\frac{\chi(\gamma - \Delta_1)}{\Delta_1 - \Delta_2}\right)$

} **Else If** ($\Delta_3 \leq \gamma \leq \Delta_4$) {

Map DOM as *Mid*

} **Else If** ($\Delta_5 \leq \gamma \leq \Delta_6$) {

Map DOM as *Late*

} **Else** {

Map DOM as 1

} **End if**

Obtain fuzzy set (Q)

Obtain crisp output (SS)

End For

Return Severity stage (SS)

End

Hence, the disease severity stages, such as early, middle, and late of the diseased leaves have been detected. Thus, the proposed model classified the type of leaf disease and checked the severity level of the disease. Therefore, in the result section, the proposed stage-wise severity prediction of the PD technique is analyzed.

4. RESULTS AND DISCUSSIONS

This segment analyzes the proposed technique's experimental results in comparison with the existing models to prove the proposed models' reliability. In the working platform of MATLAB, the experiments are performed. Figure 3 displays the sample output images,



(a)



(b)

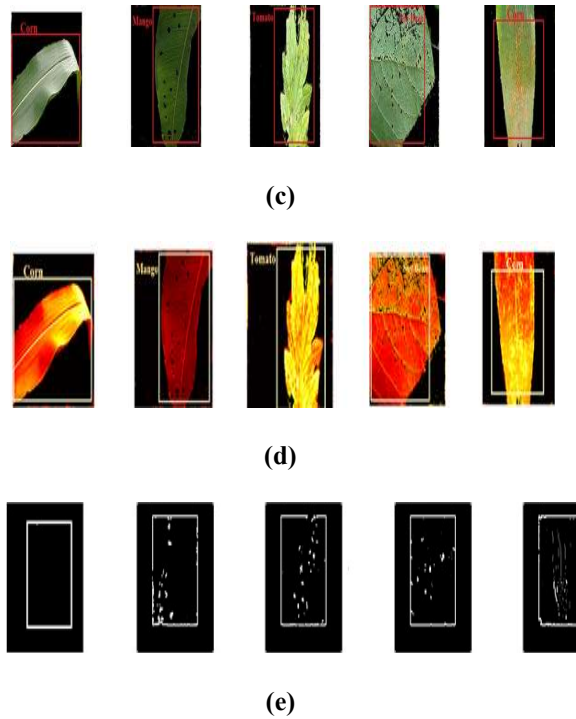


Figure 3: Sample (a) Input images, (b) Background subtracted images, (c) Labelled images, (d) fusion image of saliency mapping and labeling, and (e) ROI segmented images

4.1 Dataset description

The image data of healthy as well as disease classes of tomato and disease classes of corn are taken from the PlantDoc dataset for the experimental analysis. The image present in the PlantDoc dataset was collected by downloading it from Google Images and Ecosia. The raw images from the dataset are un-cropped images and these images are resized to 256*256 pixel size. This dataset contains leaf images from various natural environments most of which are taken during the daytime and with white or black backgrounds. Afterward, for the healthy leaf class of corn, all the classes of soybean and mango are collected from publically available sources. From the dataset, 1965 images of four plant species were collected from which 1572 images were utilized for training, whereas 393 images were willed for testing. Table 3 describes the impact of metrics evaluation in achieving enhanced plant disease classification by the proposed method.

Table 3: Performance analysis based on evaluated metrics

S. No	Metrics	Formulae	Description
1	Accuracy	$\frac{TP+TN}{TP+FP+TN+FN}$	In the formula, TP denotes true positive, TN denotes true negative, and FP denotes False positive. TP defines the correct prediction of a disease-free leaf, TN specifies the exact prediction of the diseased leaf class, and FP defines the wrong prediction of the leaf as a diseased one, which is actually disease-free, by the proposed method. The accuracy is evaluated using the respective formula. If the calculated accuracy is attained higher, it is realized that the performance is better for the proposed method than the existing methods.
2	Recall	$\frac{TP}{TP+FN}$	In the formula, FN implies a false negative, which defines how far the proposed model wrongly predicts or classifies the disease-free leaf as a diseased one. By using the formula, recall is calculated. The performance is better when the recall attains a higher value.
3	Precision	$\frac{TP}{TP+FP}$	Using the formula, the precision of the proposed work is

			evaluated. The higher precision value attained by the proposed method implies that the diseased plant images are predicted correctly.
4	F-measure	$\frac{2 * Recall * Precision}{Recall + Precision}$	F-measure is calculated using the specific formula. F-measure is the weighted average of precision and recall. The higher F-measure value implies the overall better prediction performance of the proposed model.
5	Specificity	$\frac{TN}{TN + FP}$	By using the formula, the specificity of the proposed work is calculated. The higher value of specificity attained declares how well the proposed method correctly detects the diseased class.
6	Mathew's correlation coefficient (MCC)	$\frac{(TP - FN)(FP - TN)}{\sqrt{(TP + FN)(FP + TN)(TP + FP)(TN + FN)}}$	The MCC is calculated using this formula. The higher value of MCC implies that the proposed model classifies the diseased and non-diseased plant leaves exactly.
7	Jaccard Index	$\frac{ A \cap B }{ A \cup B }$	The Jaccard Index (JI) is evaluated using this formula. In the evaluation, the higher JI value depicts how accurately the background is suppressed from

			the plant leaf image by using the proposed algorithm.
--	--	--	---

4.2 Performance analysis of severity prediction

Here, stage-wise prediction rate results of the proposed EP-Fuzzy are experimentally analyzed as follows,

Table 4: Severity Prediction Results

Class	Severity (%)		
	Early	Middle	Late
Class 1 Corn leaf spot	19.19	35.76	44.75
Class 2 Corn leaf blight	26.85	29.48	43.75
Class 3 Corn rust leaf	46.81	34.77	18.75
Class 4 Mango anthracnose	12.75	66.75	21.37
Class 5 Mango phoma blight	9.97	34.33	56.75
Class 6 Mango red rust	32.64	25	42.75
Class 7 Tomato early blight leaf	21	26.72	52.45
Class 8 Toamtoseptoria leaf spot	28.64	42.7	28.6
Class 9 Tomato Bacterial spot	40	31	28.4
Class 10 Tomato leaf late blight	21.2	54.9	24.62
Class 11 Tomato leaf mosaic virus	39.91	26.57	34.03
Class 12 Tomato leaf yellow virus	22.75	32.75	43.76
Class 13 Tomato mold leaf	33.45	68.95	8.44
Class 14 Soya bacterial spot	52.75	Nil	47.86
Class 15 Soya brown spot	23.45	38.7	37.75

Class 16 Soya cercospora leaf blight	Nil	61.86	35.45
Class 17 Soya bean rust	30.21	6	63.7

The predicted stage-wise severity levels of the diseased class leaves based on the EP-Fuzzy results are exhibited in Figure 3. Here, the severity in each class is calculated as the ratio of the number of images predicted on the corresponding stage (early, middle, and late) to the total number of images classified for the corresponding disease class. Here, 63.7% of soybean rust, 43.76% of tomato leaf yellow virus, 56.75% of mango phoma blight, and 44.75% of corn leaf spot are predicted under late-stage severity, which would affect the yield of the corresponding plant. The comparison of the proposed approach and the prevailing works is analyzed in Table 5 and Figure 4 regarding plant disease severity prediction as follows,

Table 5: Comparison of Severity Prediction

Techniques	Fuzzification Time (ms)	Defuzzification Time (ms)
Proposed EP-Fuzzy	3457	3399
Tr-Fuzzy	3761	3791
Tp-Fuzzy	3995	4011
Fuzzy	4082	4192
ANFIS	4379	4276

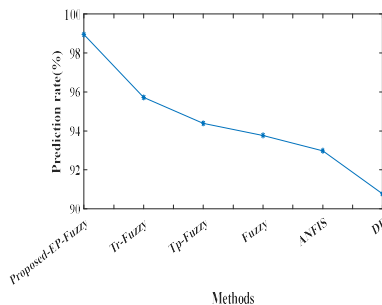


Figure 4: Comparison of Prediction Rate

The proposed EP-Fuzzy used the Exponential Pareto function as the membership function for severity prediction. Thus, the proposed model detected the severity in 98.95% Prediction Rate,

3457ms Fuzzification Time, and 3399ms Defuzzification Time. But, the existing Triangular Fuzzy (Tr-Fuzzy), Trapezoidal Fuzzy (Tp-Fuzzy), adaptive network-centric fuzzy inference system (ANFIS), and Decision Rule (DR) obtained an average of 93.53% Prediction Rate, 4181ms Fuzzification Time, and 4154ms Defuzzification Time. Thus, the proposed system achieved better results than the existing models in severity prediction of the disease.

4.3 Performance analysis of disease classification

Here, concerning the accuracy, precision, recall, F-measure, specificity, training time, and Mathews Correlation Coefficient (MCC), the proposed DRN's performance is comparatively analyzed with the Artificial Neural Network (ANN), ResNet-50, CNN, and Deep Belief Network (DBN).

Table 6: Performance Comparison of proposed DRN

Methods/Metrics	Accuracy	Recall	Precision	F-Measure	Specificity	MCC
Proposed DRN	98.34	98.22	97.19	97.7	97.16	97
ResNet-50	96.88	96.34	94.21	95.26	94.08	91
CNN	94	94.07	92.46	93.25	91.75	86
ANN	92.37	93.41	90.65	92	88.33	79
DBN	88.45	86.09	87.37	86.72	86.34	75
DNN	87.92	85.97	86.19	86.28	85.92	72
GRU	87.05	85.42	85.82	85.59	85.56	71
Bi-LSTM	85.87	84.97	85.27	84.88	84.49	69
LSTM	84.19	84.71	84.99	84.37	84.17	68
RNN	82.07	82.63	83.11	82.91	82.93	65

RBM	80.18	80.55	81.73	82.08	82.33	61
-----	-------	-------	-------	-------	-------	----

The classification performance of the proposed DRN and prevailing ResNet-50, CNN, ANN, DBN, Deep Neural Network (DNN), Gated Recurrent Unit (GRU), Bi-directional Long Short Term Memory (Bi-LSTM), Long Short Term Memory (LSTM), Recurrent Neural Network (RNN), and Restricted Boltzmann machines (RBM) methods are exemplified in Table 6. Metrics, such as Accuracy, Recall, Precision, F-Measure, Specificity, and Matthews Correlation Coefficient (MCC) were used for comparison. The proposed model obtained 98.34% Accuracy, 98.22% Recall, 97.19% Precision, 97.7% F-Measure, 97.16% Specificity, and 97% MCC. But, the existing works achieved an average of 87.89% Accuracy, 87.41% Recall, 87.18% Precision, 87.33% F-Measure, 86.59% Specificity, and 73.37% MCC. Thus, Table 6 displays that the proposed system proffered greater performance than the prevailing techniques. The graphical analysis of Table 6 has been shown as follows,

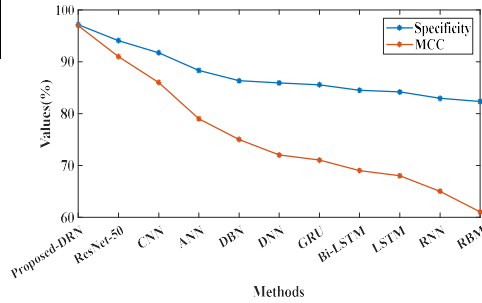


Figure 6: Specificity and MCC outcomes of classifiers

The specificity results of the proposed and the conventional classifiers are unveiled in Figure 6. Here, the ResNet-50 gives better performance than other conventional classifiers by attaining a higher specificity level of 94.08%. However, the proposed DRN overpowers the ResNet-50 by attaining a specificity value of 97.16%. Also, the MCC attained by the proposed DRN (0.97) is higher than the other conventional classifiers. Thus, this analysis proved that the proposed is more suitable for predicting single and multi-diseases in a single leaf.

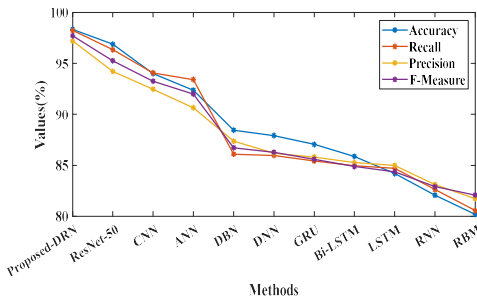


Figure 5: Classifier evaluation based on accuracy, precision, recall, and f-measure

The metrics utilized for evaluating the classifier result's quality are accuracy, precision, F-measure, and recall. Figure 5 exhibits that with the DRN, the accuracy, recall, precision, and f-measure levels are improved by 1.5%, 1.9%, 3.16%, and 2.5% than the ResNet-50 classifier. Moreover, when contrasted with CNN, ANN, DBN, DNN, GRU, Bi-LSTM, LSTM, RNN, and RBM classifiers, the proposed classifier achieved superior outcomes. Thus, the classified results of the proposed DRN are more reliable for the PD classification, even for the leaf with multiple disease classes.

Table 7: Training time analysis

Algorithms	Training time (ms)
Proposed DRN	39136
ResNet-50	43308
CNN	51846
ANN	73598
DBN	84350
DNN	87016
GRU	89963
Bi-LSTM	91702
LSTM	94781
RNN	95318
RBM	99154

As per Table 7, the training time gets reduced by 4172ms to the conventional ResNet-50 with the depth-wise convolution in the ResNet-50. But, the existing ResNet-50, CNN, ANN, DBN, DNN,

GRU, Bi-LSTM, LSTM, RNN, and RBM classifiers achieved higher training time of 43308ms, 51846ms, 73598ms, 84350ms, 87016ms, 89963ms, 91702ms, 94781ms, 95318ms, and 99154ms than the proposed DRN. This shows that the proposed DRN gives a better Multi-class leaf disease result in less time than other classifier models. Figure 7 exhibits the pictorial representation of Table 7,

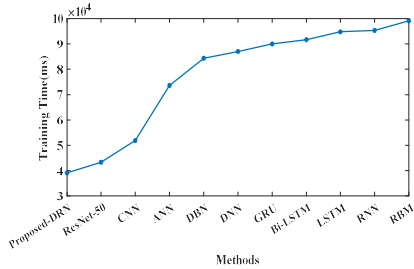


Figure 7: Training Time Analysis

Table 8: Comparison of Leaf Disease Classification

Study	Method	Accuracy	Precision	Recall	F-Measure
Proposed work	DRN	98.34	97.19	98.22	97.7
(Shewale&Daruwala, 2023)	CNN	96.7	96.1	95.5	95.45
(Divyanth et al., 2023)	UNet-DeepLabv3+	91.57	91.89	92.37	-
(Bedi & Gole, 2021)	CAE-CNN	97.38	97.72	-	-
(Prabhakar et al., 2020)	ResNet 101	94.60	-	-	90.5
(Pratap & Kumar, 2023)	EfficientNetB	92	91.05	90.86	89.25

Kumar, 2023)	4				
--------------	---	--	--	--	--

The comparison of the proposed classifier and the prevailing works is described in Table 8. In the proposed work, the features extracted after ROI segmentation were used for plant leaf disease classification. The RN classifier was replaced by Dense RN, which classified the plant leaf disease with 98.34% Accuracy, 97.19% Precision, 98.22% Recall, and 97.7% F-Measure. The existing (Shewale&Daruwala, 2023) and (Bedi & Gole, 2021) could not reject the image with a large size, which reduced the classification accuracy by 96.7% and 97.38%, respectively. The latency was not improved in (Prabhakar et al., 2020) and (Divyanth et al., 2023) works, which gave a Recall of 90.5% and a Precision of 91.89%. Also, in (Pratap& Kumar, 2023), features were not extracted, which reduced the Recall by 90.86%. Hence, by comparing the classifier result of the proposed DRN and existing classifiers, the proposed system performed better in plant disease classification.

4.4 Performance analysis of labeling

Here, the leaf labeling accuracy of the proposed SPL is analyzed in comparison with the conventional labeling models, namely PL, Generative Adversarial Network (GAN), Mix-Match (MM), and Mean Teacher (MT).

Table 9: Analysis of Labeling Accuracy

Methods	Labelling Accuracy (%)
Proposed S-PL	97.73
PL	95.09
GAN	92.33
MM	89.85
MT	87.64

The semi-supervised labeling results accuracy of proposed and conventional labeling models are demonstrated in Table 9. Here, the labeling accuracy of PL is 95.09%, which is higher than other conventional semi-supervised classifiers. However, with the Spearman technique in the PL

model, the most accurate levels of labeled data are obtained in the proposed S-PL model. Hence, the analysis has been graphically represented in Figure 8,

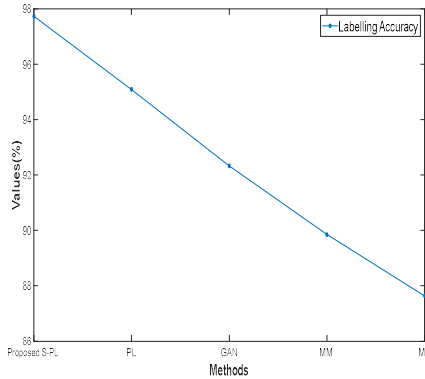


Figure 8: Labeling accuracy of semi-supervised models

4.5 Performance analysis of segmentation

Here, the proposed SC-RSM’s ROI segmentation performance is analyzed in comparison with the conventional RSM, Level Set (LS), Otsu segmentation, and Watershed (WS) techniques in terms of SA and DSC.

Table 10: DSC and SA results of segmentation

Algorithms	DSC	SA
Proposed SC-RSM	0.984	0.9824
RSM	0.953	0.9557
LS	0.917	0.9248
Otsu	0.892	0.9075
WS	0.85	0.8945

The DSC results acquired by proposed and conventional segmentation techniques are illustrated in Table 6. The DSC value near 1 represents that the system performed a better segmentation task. Here, the DSC of the proposed SC-RSM is 0.984, which is nearer to 1, whereas the other conventional segmentation techniques achieved less DSC value. From Table 10, it is prominent that the proposed SC-RSM attained a higher SA of 0.9824 than the RSM (0.9557), LS (0.9248), and Otsu (0.9075). This shows that with

the proposed SC-RSM segmentation, the ROI is segmented more accurately than other models. Table 10 has been pictorially expressed in Figure 9,

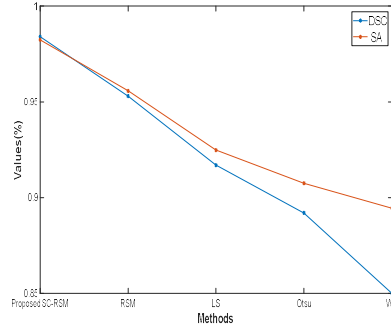


Figure 9: Performance Analysis of Segmentation

4.6 Performance analysis of background removal

Here, the proposed background subtraction technique N-GMM is experimentally analyzed in comparison with the baseline GMM, Temporal Average Filter (TAF), GrabCut (GC), and K-Means Algorithm (KMA) based on the Jaccard Index (JI).

Table 11: JI result analysis

Algorithms	JI (%)
Proposed N-GMM	96.75
GMM	94.37
TAF	91.94
GC	89.03
KMA	86.46

The JI results, which estimate the quality of the background-subtracted image, are described in Table 11. The higher JI value means that the background is removed more accurately. Here, the JI of GMM (94.37%) is higher than the other baseline techniques. However, with the proposed N-GMM, the JI is enhanced to 96.75%. This proves the efficacy of the proposed N-GMM model in the background removal in the image. The respective chart for Table 10 is shown in Figure 10.

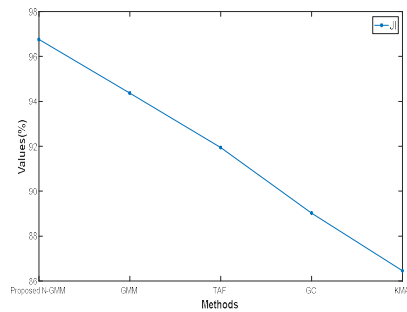


Figure 10: Analysis of JI

4.7 Comparative analysis

This phase analyzes the overall severity prediction accuracy of the proposed DRN-based EP-Fuzzy (DEF) in comparison with the existing works as described in Table 12.

Table 12: Comparison analysis

Methods	Predict ion rate (%)	Classifi cation Accuracy (%)	Classifi cation Recall (%)
Proposed DEF	96.26	98.34	98.22
ResNet-101[26]	94.6	94.60	-
Fuzzy [20]	94.33	91.59	94.4
VGG-16 [21]	95.33	89	-
FCM-CSA [24]	94.23	91.67	93.56
CAE-CNN [25]	93.21	97.38	97.72
CNN [30]	94.1	96.7	96.1
UNet-DeepLabv3+ [18]	90.86	91.57	91.89
EfficientNetB4 [17]	91.5	92	91.05
SPA-RF [14]	93	95.1	-
CNN [19]	94	93	95

Concerning prediction accuracy, the comparative analysis of the proposed and the existing models is

exemplified in Table 12. The prediction accuracy is estimated by combining the class prediction results with the DRN classifier and EP-Fuzzy severity prediction. Here, the proposed technique attains a higher prediction rate (98.26%) than the existing ResNet-101, Fuzzy, VGG-16, FCM-CSA, CAE-CNN, CNN, UNet-DeepLabv3 +, EfficientNetB4, and SPA-RF models. Also, the plant disease classification was done by the proposed DBN model, which classified the type of disease with an Accuracy of 98.34% and Recall of 98.22%. Most of the existing works have not concentrated on the background removal of the image and feature extraction. Some related works have considered single disease classification or one plant type for disease prediction. Thus, the existing works obtained lower metric values of prediction rate, Accuracy, and Recall than the proposed work. This shows that with the proposed framework, the single or multiple disease severity stages in multiple plant leaves can be predicted effectively.

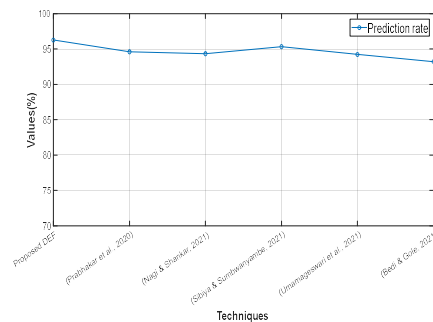


Figure 11: Comparative analysis with existing works

Figure 11 depicts the comparison of the proposed DRN-based EF-Fuzzy algorithm and existing works regarding the severity prediction rate. The proposed work predicted the severity of plant leaf disease better than the existing models.

4.8 Summarization and Discussion

In this section, the overall performance of the proposed work with respect to techniques, such as EP-Fuzzy, DRN, S-PL, N-GMM, and SC-RSM is described in detail. First, the background from the input image was subtracted using the N-GMM model. The sub-pixels were automatically recognized by the model and thus extracted the background in 96.75% JI as given in Table 11. The data was then augmented and leaf labeling was done using the S-PL technique with a labeling accuracy of 97.73%, which is depicted in Figure 8.

The leaf-labeled image was then mapped, and along with the mapped image, the labeled image was segmented using the SC-RSM technique in 0.9824 SA as displayed in Table 10. The important features were then extracted and classified using the DRN method. Thus, the segmented image was classified into types of disease with 98.34% Accuracy, 98.22% Recall, and 97.19% Precision, which is described in Table 6. The classified images were then given for disease severity prediction using the EP-Fuzzy algorithm and this method predicted the plant leaf disease with a 96.26% Prediction rate as exhibited in Figure 4. Hence, the proposed framework classified the type of plant leaf disease accurately and predicted the severity of the plant disease effectively. In large-scale farming operations, monitoring of entire plant is time-consuming. Hence, multi-disease prediction using image data reduces the time complexity with accurate output. To increase the accuracy, this research work proposed an advanced method. This monitoring process is also helpful in agriculture and food production industrial applications.

4.9 Contribution vs. Limitation

In the proposed framework, the background of the image was extracted and then augmented to improve the quality of the image. Multiple plant leaves were taken for disease prediction in this work, whereas the existing models mostly concentrated on a single plant for disease prediction. Also, the prevailing works did not concentrate on important features for disease classification. So, in this work, features from the segmented images were extracted and given to the classifier for accurate classification. Multi-disease was classified, and from that, the severity of the disease was also predicted. However, the disease was predicted only in the leaf of a plant and not on the whole plant. So, the enhancement of the work will be done by predicting disease in other parts of the plant.

4.10 Strengths and Weakness of the Study

The presented research work concentrates on the multi-class plant leaf disease classification and severity stage identification. The research work has some strengths and weaknesses, which are discussed here. The research is highly helpful for the leaf, which is affected by more than one disease. The severity stage identification helps understand how the disease is spread in the plant and know the urgency of the treatment. The

classification of multi-leaf disease prediction and severity assessment of the multi-leaf disease enables precision management of crop health. However, the research generally concentrates on specific leaves but different varieties of leaves are presented under the selected plant. The research work is also only suitable for corn, mango, tomato, and soya plants. The diseases are also predicted in the leaves of a plant and not in the whole plant.

5. CONCLUSION

This paper proposed an effective DEF-based single and multi-disease in a single leaf of tomato, corn, soybean, and mango. Here, semi-supervised S-PL-based leaf labeling was performed to avoid misclassification of multi-class diseases in plant leaves. The proposed approaches are experimentally analyzed on the image data collected from publicly available sources. The complex background, which would affect the prediction performance, was removed using the N-GMM method. In experimental assessment, the N-GMM model achieved a JI rate of 96.75%, which is higher than the existing methods. Then, the data augmentation was conducted for the background extracted image to improve the quality of the image. Multi-leaf disease class was focused on in the proposed work. Hence, the labeling of the leaves was done using the S-PL technique. The labeled method attained 97.73% labeling accuracy in experimental analysis. Next, to predict the multi-class disease in a plant leaf, the leaf image was segmented using the SC-RSM technique. Here, for segmentation, the labeled image and salience-mapped images were given as input. The experimental outcome shows that the SC-RSM achieved 0.984 of DSC and 0.9824 of SA, which are higher than the existing methods. After segmenting, the types of plant leaf disease were classified using the DRN classifier. The DRN achieved 98.34% accuracy and less training time because of handling the removal of complex backgrounds and accurate labeling of leaf images. Finally, the severity of the plant leaf disease was predicted using the EP-Fuzzy algorithm. The EP-Fuzzy method took lesser fuzzification and defuzzification time compared with the existing methods. Overall, the proposed multi-leaf labeling, background removal, data augmentation, and segmentation approaches achieved better performance than the conventional approaches. Also, compared with the state-of-the-art works, the proposed disease prediction approach DEF achieved a 96.26% prediction rate, 98.34%

classification accuracy, and 98.22% classification recall. The obtained outcomes are higher than the state-of-the-art works because the proposed research work concentrates on all the main factors of disease classification. Thus, it is concluded that the proposed model classified the multi-class plant leaf disease effectively for multi-leaves and predicted the severity of the disease.

Future Scope

Although the proposed work classified and predicted the plant leaf disease accurately, only four kinds of plants like corn, mango, tomato, and soya were considered in this work. Also, the disease present in other parts of the plant was not taken into account. Therefore, in the future, several other plants will be considered and the disease present in other parts of the plant like stem and fruit will also be included to enhance the performance of the model.

Declarations:

Conflict of interest: The authors declare that they have no conflict of interest.

Ethical approval: This article does not contain any studies with human participants or animals performed by any of the authors.

Consent of publication: Not applicable.

Availability of data and materials: Data sharing is not applicable to this article as no datasets were generated or analyzed during the current study.

Competing interests: The authors declare that they have no competing interests

Funding: This work has no funding resource.

Author's contributions: All authors contributed to the study conception and design. Material preparation, data collection and analysis were performed by ¹D. Lita Pansy, ²Dr.M.Murali. The first draft of the manuscript was written by ¹D. Lita Pansy and all authors commented on previous versions of the manuscript. All authors read and approved the final manuscript.

Acknowledgement: We thank the anonymous referees for their useful suggestions.

REFERENCES

- [1] T. Domingues and T. Brandao, "Machine Learning for Detection and Prediction of Crop Diseases and Pests: A Comprehensive Survey", *Agriculture*, 2022, pp. 1–23.
- [2] T. Shi, Y. Liu, X. Zheng, K. Hu, H. Huang, H. Liu and H. Huang, "Recent advances in plant disease severity assessment using convolutional neural networks", *Scientific Reports*, Vol. 13, No. 1, pp. 2336, 2023.
- [3] K. P. Akshai, and J. Anitha. "Plant disease classification using deep learning", 3rd International Conference on Signal Processing and Communication (ICPSC), 2021, pp. 407–411.
- [4] Y. Liu, G. Gao, and Z. Zhang, "Crop disease recognition based on Modified Light-Weight CNN with attention Mechanism", *IEEE Access*, Vol. 10, 2022, pp. 112066–112075.
- [5] K. Garg, S. Bhugra, and B. Lall, "Automatic Quantification of Plant Disease from Field Image Data Using Deep Learning", *Proceedings - 2021 IEEE Winter Conference on Applications of Computer Vision, WACV*, 2021, pp. 1964–1971.
- [6] K. S. Alves , M. Guimarães, J. P. Ascari, M. F. Queiroz, R. F.Alfenas, E. S. G. Mizubuti, and E. M. Del Ponte, "RGB-based phenotyping of foliar disease severity under controlled conditions", *Tropical Plant Pathology*, Vol. 47, No. 1, 2021, pp. 105–117.
- [7] C. H. Bock, "Plant disease severity estimated visually : a century of research , best practices , and opportunities for improving methods and practices to maximize accuracy", *Tropical Plant Pathology*, 2022, pp. 25–42.
- [8] A. Wang, P. Du, H. Wu, J. Li, C. Zhao, and H. Zhu, "A cucumber leaf disease severity classification method based on the fusion of DeepLabV3+ and U-Net", *Computers and Electronics in Agriculture*, Vol. 189, 2021, p. 106373.
- [9] L. He, S. Qi, J. Duan, T. Guo, W. Feng, and D. He, "Monitoring of Wheat Powdery Mildew Disease Severity Using Multiangle Hyperspectral", *IEEE Transactions on Geoscience and Remote Sensing*, Vol. 59, No. 2, 2020, pp. 979-990.
- [10] Z. Chen, R.Wu, Y. Lin, C. Li, S. Chen, Z. Yuan, S. Chen, and X. Zou, "Plant Disease Recognition model based on improved YOLOV5", *Agronomy*, Vol. 12, No. 2, 2022, pp. 1-14.

- [11] K. V. Prasad, H. Vaidya, C. Rajashekhar, K. S. Karekal, R. Sali, and K. S. Nisar, "Multiclass classification of diseased grape leaf identification using deep convolutional neural network(DCNN) classifier", *Scientific Reports*, Vol. 14, No. 1, pp. 1-13, 2024.
- [12] Y. Li, X. Chen, L. Yin, and Y. Hu, "Deep Learning-Based Methods for Multi-Class rice Disease Detection using plant images", *Agronomy*, Vol. 14, No. 9, 2024, pp. 1-19.
- [13] M. V. Shewale and R. D. Daruwala, "High performance deep learning architecture for early detection and classification of plant leaf disease", *Journal of Agriculture and Food Research*, Vol. 14, 2023, pp. 1-9.
- [14] X. Jiang, J. Zhen, J. Miao, D. Zhao, J. Wang, and S. Jia, "Assessing mangrove leaf traits under different pest and disease severity with hyperspectral imaging spectroscopy", *Ecological Indicators*, Vol. 129, 2021, pp. 1–13.
- [15] X. Jiang, J. Zhen, J. Miao, D. Zhao, Z. Shen, J. Jiang, C. Gao, G. Wu, and J. Wang, "Newly-developed three-band hyperspectral vegetation index for estimating leaf relative chlorophyll content of mangrove under different severities of pest and disease", *Ecological Indicators*, Vol. 140, 2022, pp. 1–14.
- [16] S. Afzal, M. A. Tariq, A. Khanum, A. Haroon, M. A. Hussain, A. U. R. Chaudary, M. Batool, M. A. Bashir, R. Alajmi, M. Essa, S. Ejaz, and S. Samreen, "Grasp of wheat leaf rust through plant leaves extract and bioagent as an eco-friendly measure", *Journal of King Saud University - Science*, Vol. 35, No. 2, 2023, pp. 1–6.
- [17] V. K. Pratap and N. S. Kumar, "High-precision multiclass classification of chili leaf disease through customized EfficientNetB4 from chili leaf images", *Smart Agricultural Technology*, Vol. 5, 2023, pp. 1–11.
- [18] L. G. Divyanth, A. Ahmad, and D. Saraswat, "A two-stage deep-learning based segmentation model for crop disease quantification based on corn field imagery", *Smart Agricultural Technology*, Vol. 3, 2023, pp. 1-12.
- [19] H. D. Mafukidze, G. Owomugisha, D. Otim, A. Nechibvute, C. Nyamhere, and F. Mazunga, "Adaptive thresholding of CNN features for maize leaf disease classification and severity estimation," *Applied Sciences*, Vol. 12, No. 17, 2022, pp. 1-22.
- [20] R. Nagi and S. S. Tripathy, "Severity Estimation of Grapevine Diseases from Leaf Images Using Fuzzy Inference System", *Agricultural Research*, Vol. 11, No. 1, 2021, pp. 112–122.
- [21] M. Sibiya and M. Sumbwanyambe, "Automatic Fuzzy Logic-Based Maize Common Rust Disease Severity Predictions with Thresholding and Deep Learning", *Pathogens*, Vol. 10, No. 2, 2021, pp. 1–17.
- [22] Y. Zhao, J. Chen, X. Xu, J. Lei, and W. Zhou, "SEV-Net: Residual network embedded with attention mechanism for plant disease severity detection", *Concurrency and Computation Practice and Experience*, Vol. 33, No. 10, 2021, pp. 1-18..
- [23] S. Xiang, Q. Liang, W. Sun, D. Zhang, and Y. Wang, "L-CSMS: novel lightweight network for plant disease severity recognition", *Journal of Plant Diseases and Protection*, Vol. 128, No. 2, 2021, pp. 557–569.
- [24] A. Umamageswari, N. Bharathiraja, and D. S. Irene, "A Novel Fuzzy C-Means based Chameleon Swarm Algorithm for Segmentation and Progressive Neural Architecture Search for Plant Disease Classification", *ICT Express*, Vol. 9, No. 2, 2021, pp. 160–167.
- [25] P. Bedi and P. Gole, "Plant disease detection using hybrid model based on convolutional autoencoder and convolutional neural network", *Artificial Intelligence in Agriculture*, Vol. 5, 2021, pp. 90–101.
- [26] M. Prabhakar, R. Purushothaman, and D. P. Awasthi, "Deep learning based assessment of disease severity for early blight in tomato crop", *Multimedia Tools and Applications*, Vol. 79, No. 39–40, 2020, pp. 28773–28784.
- [27] P. Wspanialy and M. Moussa, "A detection and severity estimation system for generic diseases of tomato greenhouse plants", *Computers and Electronics in Agriculture*, Vol. 178, 2020, pp. 1-13.